

Modeling of Rock Friction

1. Experimental Results and Constitutive Equations

JAMES H. DIETERICH

U.S. Geological Survey, Menlo Park, California 94025

Direct shear experiments on ground surfaces of a granodiorite from Raymond, California, at normal stresses of ~ 6 MPa demonstrate that competing time, displacement, and velocity effects control rock friction. It is proposed that the strength of the population of points of contacts between sliding surfaces determines frictional strength and that the population of contacts changes continuously with displacements. Previous experiments demonstrate that the strength of the contacts increases with the age of the contacts. The present experiments establish that a characteristic displacement, proportional to surface roughness, is required to change the population of contacts. Hence during slip the average age of the points of contact and therefore frictional strength decrease as slip velocity increases. Displacement weakening and consequently the potential for unstable slip occur whenever displacement reduces the average age of the contacts. In addition to this velocity dependency, which arises from displacement dependency and time dependency, the experiments also show a competing but transient increase in friction whenever slip velocity increases. Creep of the sliding surface at stresses below that for steady state slip is also observed. Constitutive relationships are developed that permit quantitative simulation of the friction versus displacement data as a function of surface roughness and for different time and velocity histories. Unstable slip in experiments is controlled by these constitutive effects and by the stiffness of the experimental system. It is argued that analogous properties control earthquake instability.

INTRODUCTION

The principal source of uncertainty and variability found in theories for the earthquake source is the designation of mechanical properties to represent interactions along a fault prior to and during an earthquake. It is asserted here that physical parameters and phenomena observed in laboratory fault friction experiments provide a rational means for identifying the mechanical properties controlling fault slip.

Of course, faults as studied in the laboratory do not have many of the complexities of natural faults. It could be argued therefore that important controlling processes that operate in natural fault systems have been simplified out of the experiments. However, there exist many analogies between the response of simple laboratory faults and real fault phenomena—a situation that invites detailed analysis of laboratory fault friction processes for possible application to faulting. The most widely noted analogy is the possible relevance of unstable frictional sliding (stick slip) to the mechanism of crustal earthquakes caused by unstable fault slip [Brace and Byerlee, 1966]. In addition to the qualitative similarities between stick slip and earthquake fault slip, Dieterich [1974] proposes that stick slip can account for the relatively low stress drops of earthquakes when differences in slip distribution on experimental surfaces (relatively uniform slip along the entire surface) and earthquake faulting (nonuniform slip on a confined patch) are taken into account. Similarly, experimental observations of stable frictional slip have been equated with aseismic fault creep [Scholz *et al.*, 1969]. Elevated temperatures are found to enhance the tendency for stable sliding and may account for the absence of earthquakes below 15 km in California [Brace and Byerlee, 1970]. A test of the use of friction data to earthquake faulting was provided by the earthquakes at Rangely, Colorado. It was found that the Rangely earthquakes could be accounted for and modeled [Dieterich *et al.*, 1972] at the stresses and fluid pressures, measured in the focal zone [Raleigh *et al.*, 1972] using friction data for the onset of slip as

a function of confining pressure and fluid pressure [Byerlee, 1975]. At a more speculative level, observations of time-dependent friction have been used to explain the mechanism of aftershocks [Dieterich, 1972a], and experimental observations of preseismic slip may explain certain earthquake precursors [Dieterich, 1978a].

The general insensitivity of friction measurements to rock type, test conditions, and characteristics of the sliding surface further suggests that laboratory friction may be relevant to natural faults under more complex conditions. Similar values for the coefficient of friction and qualitatively similar slip phenomena are obtained for slip on clean, machine-finished surfaces and on surfaces with simulated gouge and for slip on fracture surfaces. This indicates that the processes controlling the coefficient of friction and slip instability are intrinsic to slip on discontinuities in rocks and are not greatly dependent on complexities of geometry, structure, or composition.

Instability theories for the earthquake source have an essential feature in common. Some form of displacement (or strain) weakening for the fault or focal region is generally postulated to give rise to the instability and stress drops of earthquakes. However, little attention has been given to the mechanism causing displacement weakening. For repeated slip along a fault the requirement of displacement weakening has a corollary—some type of healing mechanism must operate to restore the fault strength following earthquake slip. Otherwise, the fault strength would eventually fall to zero with repeated earthquakes.

The purpose of this paper is to (1) present experimental data that are relevant to understanding displacement weakening and healing processes, (2) develop constitutive equations that account for the experimental details, and (3) discuss some implications of the results for slip instability and earthquake faulting. The companion paper [Dieterich, 1979] employs the constitutive equations to model experimental observations of preseismic fault slip.

PREVIOUS WORK

The friction model and constitutive relationships developed in a later section of this paper extend the results of Dieterich

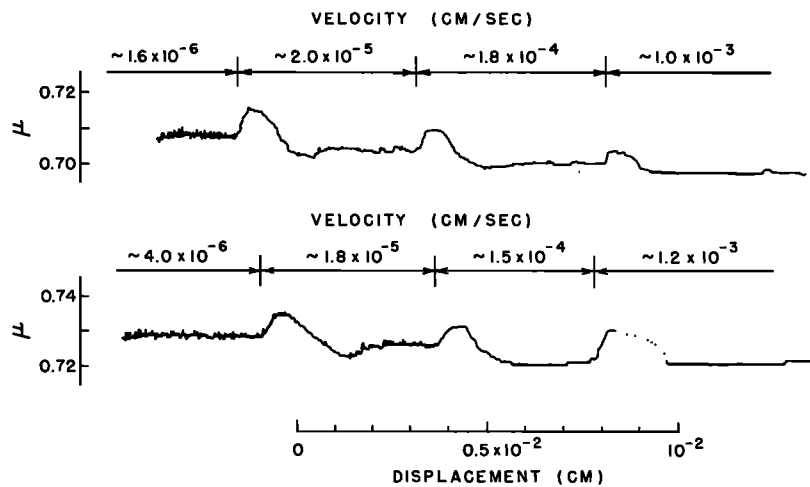


Fig. 1. Coefficient of friction μ versus displacement. Slip velocities are shown by the arrows above the experimental curves.

[1978b] on time dependence and velocity dependence of friction and displacement weakening effects. Earlier observations showing time dependence of friction [Dieterich, 1972b; Scholz et al., 1972; Teufel and Logan, 1978] give convincing evidence on the characteristics of fault healing in friction experiments. It is found that the coefficient of static friction increases with the time of stationary contact. The following empirical law has been proposed [Dieterich, 1978b] for the time dependency:

$$\mu = \mu_0 + A \log (Bt + 1) \quad (1)$$

where μ is the coefficient of friction given by the ratio of shear to normal stress, τ/σ ; t is the time of contact measured in seconds; and μ_0 , A , and B are constants with values of approximately 0.6–0.8, 0.01–0.02, and 1.0–2.0, respectively. Measurement of sliding friction at different velocities of slip [Dieterich, 1978b] has shown an analogous velocity dependency:

$$\mu = \mu_0 + A \log [B(d_c/\delta) + 1] \quad (2)$$

where d_c is an experimental displacement parameter and δ is slip velocity. Hence friction decreases with increasing slip velocity. Note that (2) is equal to (1) if the constants μ , A , and B are the same and time t is replaced by

$$t = d_c/\delta \quad (3)$$

Displacements and velocities are in centimeters and centimeters per second, respectively. The identification of the parameter d_c was suggested by records giving friction as a function of displacement. Those records show that if the slip velocity is increased, the coefficient of friction does not drop immediately to a value characteristic of the new slip velocity but that the friction changes with displacement and stabilizes at the lower value only after a critical displacement, d_c , has taken place. The magnitude of d_c appears to be independent of the magnitude of the change of velocity but does correlate with surface roughness. Values of approximately 5×10^{-4} cm and 1×10^{-4} cm were obtained for surfaces lapped with #240 and #600 abrasives, respectively, independent of normal [Dieterich, 1978b].

These observations were interpreted [Dieterich, 1978b] to be of importance in understanding the surface interactions that control friction and cause slip instability. The dependence of d_c on surface roughness and the apparent success of using (3) to replace time in (1) suggest that the t in (3) is properly the average lifetime of a population of contacts and that d is the

displacement required to change the population of contact points completely. Hence the friction observations noted above can be interpreted to result from the competition of two distinct processes. First, as a population of contacts ages, friction increases according to (1). Second, displacement acts to destroy an existing population of contacts, which is then replaced with new and consequently weaker contacts. Displacement weakening occurs whenever the average lifetime of the population of contacts decreases because of displacement.

On the basis of this interpretation a simple spring and slider model was proposed to explain experimental observations of the transition from stable sliding to stick slip [Dieterich, 1978b]. The principal shortcoming of the model is that it does not predict or account for laboratory observations of pre-seismic slip. Modeling of pre-seismic slip, which is discussed in the companion paper, appears to require a more complete constitutive relationship for friction as a function of displacement, velocity, and time. The procedure followed below is to build up constitutive equations that permit detailed simulation of experimental records for μ for different time, displacement, and velocity conditions. The model, which is discussed more fully later in this paper, quantitatively accounts for experimental observations that show that the transition from stable to unstable slip depends on normal stress, stiffness, and surface roughness. Further, it is expected that such constitutive relationships will find application for analysis of the earthquake instability.

EXPERIMENTAL RESULTS AND CONSTITUTIVE EQUATIONS

The experimental results presented here were obtained using the 'sandwich' type direct shear configuration described previously [Dieterich, 1972b]. The sample material is granodiorite from the Raymond, California, quarry. Sliding surfaces were lapped using #60, #240, or #600 abrasive.

Figure 1 gives results for the coefficient of friction, μ , as a function of displacement. Normal stress was held constant at 6.07 MPa. For each of the two experimental runs shown in Figure 1, slip velocity varied in a stepwise manner from $\sim 10^{-6}$ cm/s to $\sim 10^{-3}$ cm/s. Each curve represents a continuous record in which the velocity of slip was held constant for a displacement of $\sim 5 \times 10^{-3}$ cm, abruptly increased by a factor of 10, and held constant for another displacement of $\sim 5 \times 10^{-3}$ cm, and so on. The small irregularities in the experimen-

TABLE 1. Center-Line-Average Surface Roughnesses and Critical Displacements

Surface	Roughness, $\times 10^{-4}$ cm	$d_c, \times 10^{-4}$ cm
#60	~ 6.0	10-24
#240	~ 0.7	5-15
#600	~ 0.15	1-3

tal curves are caused by electronic noise. The apparently greater noise at the slower sliding velocities arises because of lower recording pen velocity, which compresses the irregularities on the record. In Figure 1, note that μ stabilizes at progressively lower values for each increase in sliding velocity as indicated by (2). The transient increase in μ , observed when the velocity is increased, is discussed below. Critical displacement d_c for slip on the #60 surfaces shown in Figure 1 is taken to be $\sim 2 \times 10^{-3}$ cm. Table 1 lists the center-line-average surface roughnesses and critical displacements for the #60, #240, and #600 surfaces.

As shown by Table 1 there exists a good correlation between surface roughness and the magnitude of d_c . Hence d_c may be directly related to the height or size of contacting asperities. However, wear-generated gouge is developed between the surfaces. This raises the possibility that d_c is controlled instead by either gouge thickness or maximum particle size in the gouge. Both the particle size and thickness of the gouge appear to increase as a function of the initial surface roughness.

Figure 2 gives μ as a function of displacement for a different type of experiment with the #60 surfaces. In these experiments the driving ram was held stationary for approximately 400 s and then advanced at different velocities as shown at the top of the figure. Normal stress was held constant at 5.72 MPa. The peak of the curve gives the 'static' friction. These experiments show that static friction is sensitive to loading rate—a feature that had not been noted previously. Higher rates of loading give higher static friction values. This effect appears to be analogous to the well-known effect of strain rate on critical stress for yield or fracture of silicates. It will be shown that this effect is probably related to the transient increase in μ when velocity is increased as shown by Figure 1. Note again in Fig-

ure 2 that the change in friction takes place over a characteristic displacement and that sliding friction tends to stabilize at lower values for the higher slip velocities. The points on the curves labeled o.v. and c.v. correspond to the opening and closing, respectively, of the hydraulic valve that controls motion of the driving ram. The jump in the curve at c.v. probably arises because of a slight pressure surge in the hydraulic system. Small amounts of fault creep that partially relax stress in the sample cause the decrease in amplitude of the curves between c.v. and o.v. During creep the rate of slip rapidly decays with time. Previously, Johnson [1975] reported a similar surface creep phenomena at stresses below the nominal stress for static friction and having a slip velocity that decays with time. Additionally, this creep appears to be related to the primary fault creep studied by Solberg *et al.* [1978]. That the creep takes place at stresses below the stresses for steady state slip (equation (2)) is believed to be caused by the same process that gives higher peak friction values at higher loading rates. These phenomena will be discussed more fully below.

For the purposes of developing a more complete constitutive relation for friction it is assumed that friction of rocks, like friction of metals and most other materials, is largely controlled by adhesion at actual points of contact between sliding surfaces directly or between gouge particles separating the surfaces. Several lines of evidence indicate that adhesion is the principal source of the frictional force in rocks [Dieterich, 1978b]. Reliance on adhesion is not essential for the following discussion; however, it does provide a plausible framework for discussion of parameters and for interpretation of mechanisms.

Bowden and Tabor [1964] propose that when surfaces are brought into contact, minute irregularities will prevent uniform contact over the entire surface, even for flat, well-polished surfaces. Actual contact is limited to scattered points (asperities) where the contact stresses are very high. An increase of the normal stress pushing the surfaces together causes the points of contact to yield and results in an increase of the real area of contact. For a unit area of surface, the real area of contact A may be approximated by

$$A = C\sigma \quad (4)$$

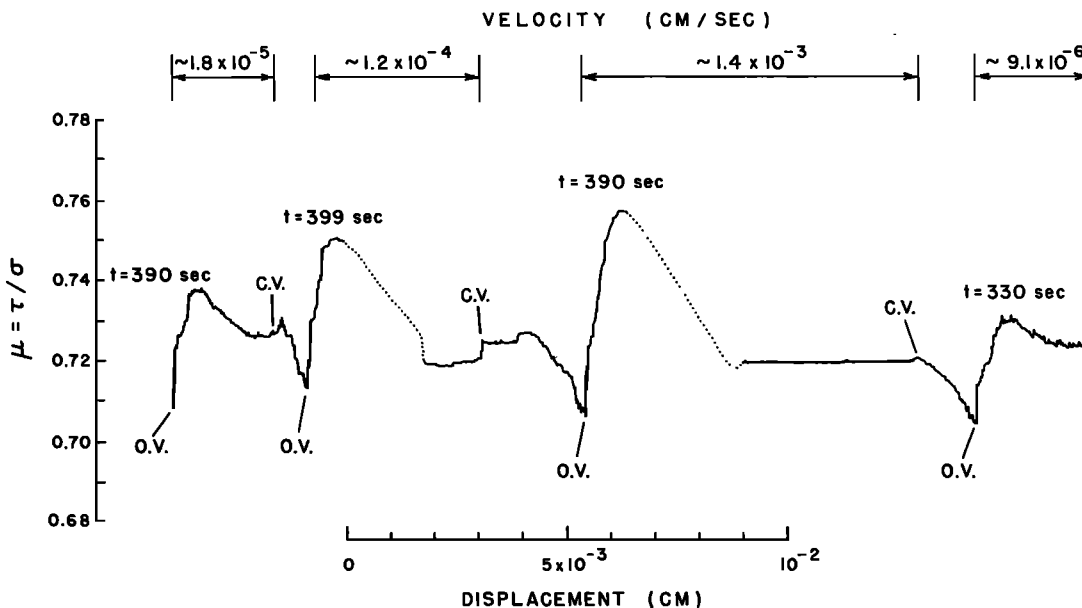


Fig. 2. Coefficient of friction versus displacement. The driving ram was held fixed for 400 s and then advanced at the velocities indicated above the experimental curve.

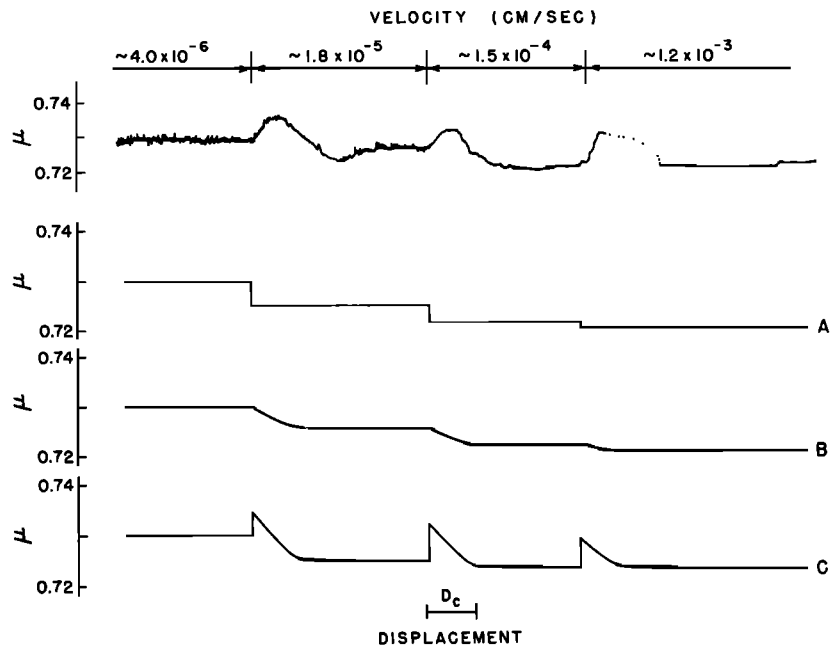


Fig. 3. Comparison of experimental results from Figure 1 with empirical friction laws. Curve A employs (3) and (8), with $c_1F = 0.72$, $c_2F = 0.005$, and $c_3 = 0.1$. Curve B employs (8) and (9). Curve C employs (9) and (11), with $d_c = 2 \times 10^{-3}$ cm, $c_1 = 0.69$, $c_2 = 0.010$, $c_3 = 0.5$, $f_1 = 1.0$, $f_2 = 25.$, and $f_3 = 2 \times 10^{-3}$.

where σ is the average normal stress applied over the entire surface (assuming 100% contact) and C is a material constant inversely proportional to indentation hardness or yield stress. Bowden and Tabor assert that the resistance of the surface to slip is controlled by the adhesive strength of the junctions. Hence the average shear stress τ (again assuming uniform contact) for slip is proportional to the real area of contact:

$$\tau = FA \quad (5)$$

where F is the strength per unit area of a contact. The coefficient of friction, μ , is given by τ/σ :

$$\mu = \tau/\sigma = CF \quad (6)$$

Note that $C \times F$ is dimensionless because C^{-1} and F are proportional to strength. A significant implication of this analysis is that stresses at points of contact are independent of the applied normal stress.

The time dependence of (1) is clearly related to an increase in area of contact, or perhaps, in some situations, depth of penetration of asperities [Scholz and Engelder, 1976; Teufel and Logan, 1978; Dieterich, 1978b]. In response to the high stresses in the vicinity of the contact points, creep deformation occurs, causing the increase in area. This suggests that C in (4) is time dependent:

$$C = c_1 + c_2 \log(c_3 t + 1) \quad (7)$$

giving for the coefficient of friction from (6):

$$\mu = [c_1 + c_2 \log(c_3 t + 1)][F] \quad (8)$$

which is the same as (1) with $c_1F = \mu_0$, $c_2F = A$, and $c_3 = B$.

The reader will note that (8) applies to static friction if t is the time of stationary contact or to sliding friction if t is the average lifetime of the population of contacts. The use of (8) with relationship (3) for the average time of contact as a function of velocity gives a steplike change in friction whenever the sliding velocity abruptly changes. Figure 3, curve A, is a simulation of the experimental run (top curve) using (3) and (8). Comparison of curve A with the experimental results

demonstrates the unsuitability of this approach for accurate representation of friction as a function of displacement. The steps in curve A arise because t is assumed to jump to a new value whenever the velocity changes. The observations suggest, however, that t relaxes to the new value over the characteristic displacement d_c . A relationship that satisfactorily represents the relaxation of t as a function of displacement δ is given by

$$t = \frac{d_c}{\delta} \left(\frac{\delta}{d_c} t_0 \right)^{\exp((\delta_0 - \delta)/d_c)} \quad (9)$$

where t_0 and δ_0 are the average contact time and displacement, respectively, when the slip velocity is changed to the new value. Use of (9) with (8) for step changes in velocity gives curve B of Figure 3. For slip histories with variable velocities, (9) permits a continuous representation of t as a function velocity and displacements for arbitrarily small displacement steps.

The transient increase in friction observed when the velocity is increased seems not to be associated with variation of surface area with displacement but appears to result from another process. The interpretation is offered here that this effect results from a loading rate dependence of the strength term, F . The following relationship appears to give satisfactory results:

$$F = f_1 + \frac{1}{f_2 \log[(f_3/\delta) + 10]} \quad (10)$$

where f_1 , f_2 , and f_3 are constants. For the simulations discussed here and in the companion paper, f_3 has been equated with d_c . Several other relationships might serve as well. The essential characteristic of (10) is that if the area of contact is held constant, the strength of a contact increases as the velocity of loading increases. As noted above, this observation agrees with the effect of strain rate on yield strength usually observed for silicates. In addition, it is noted that the creep that apparently causes the time-dependent increase in area (equation (7)) implies a similar strain rate dependence in strength. In the former case the deformation is in response to the normal stress, while the latter case arises in response to shear.

Use of (10) and (7) gives the following expression for the coefficient of friction as a function of velocity and time of contact:

$$\mu = [c_1 + c_2 \log(c_3 t + 1)] \left\{ f_1 + \frac{1}{f_2 \log [(f_3/\dot{b}) + 10]} \right\} \quad (11)$$

Equation (11) used with (9) for the variation of contact time with displacement and velocity appears to represent adequately the static, transient, and steady state sliding friction observations described above.

Curve C in Figure 3 gives the variation of μ as a function of displacement and velocity using (11) and (9). Overall, curve C appears to be in good agreement with the data. An increase in sliding velocity first causes an increase in friction because of the velocity dependence of F . As sliding proceeds, however, the average time of contact relaxes to the new value, causing a decrease in the real area of contact and an overall lowering of the total resistance to slip. In detail, the simulation shown by curve C (Figure 3) differs from the experiments, mainly in the sharp peak in friction obtained when the velocity is increased.

Figure 4 shows further refinement of the simulation that tends to smooth out the peaks. In this simulation the velocity of slip accelerates and temporarily overshoots the driving velocity. This type of velocity overshoot is evident in the displacement versus time records for the experiments and apparently arises because of elasticity of the sample and load-bearing anvils in the apparatus. For this simulation the experiment was broken into small displacement steps, and the velocity history given by curve C was used with (9) to obtain t and μ at the end of each step.

Figure 5 gives a simulation of the experiment shown in Figure 2 for static friction as a function of loading velocity. Again, (11) was used to determine μ . The initial time of static contact was taken to be 400 s, and (9) was used to give the variation of contact time with displacement and velocity. Comparison of Figure 5 with Figure 2 shows that the simulation provides a reasonably good quantitative representation of principal features of the experiment. No attempt was made

here to represent the variations in slip velocity due to elastic effects in the apparatus or to model the fault creep that occurred in the experiments when the hydraulic system feeding the driving ram was valved off. Incorporation of a more realistic velocity history that accounts for accelerations of slip rates when the surface begins to slide would result in flattening of the peaks in the friction curves and yield a better agreement with the experimental curves.

Fault creep (c.v. to o.v. in Figure 2) with displacement rates that decay with time giving time-displacement curves resembling transient creep is observed at stresses below the coefficient of friction for steady state slip (i.e., when \dot{b} is constant and displacement is sufficiently large for $t = d_c/\dot{b}$). This effect can be accounted for by (11) and arises because of the velocity dependence of F . The characteristics of fault creep observed in the experiments of Figure 2 are illustrated with the aid of Figure 6. Figure 6 plots μ from (11) against the logarithm of the contact time for different velocities of slip. Constants for C , F , and d_c are those used for the above simulations. The heavy dashed curve in Figure 6 gives μ as a function of contact time assuming $t = d_c/\dot{b}$. Hence the dashed curve gives the value for μ and t for steady state slip at constant velocity. During slip at constant velocity, if the parameters for μ and t fall on the dashed curve, those parameters will be stable and will not change unless \dot{b} is changed. If the conditions during slip plot above the dashed curve, then slip will be at a velocity in excess of the steady state velocity and therefore cause a decrease in t with displacement. In this case, if the velocity of slip is held constant, then t and consequently μ must decrease with displacement until both parameters coincide with the steady state values. On the other hand, if the stress is held constant above the dashed curve, then acceleration of slip must result to compensate for the decrease in contact time. This may explain the observation of tertiary creep leading to unstable slip reported by Solberg *et al.* [1978]. Similarly, slip may take place for conditions plotting below the dashed curve. In this case the velocity of slip is less than the steady state value, and t must increase as a result. If velocity is held constant, μ will increase with t along a velocity contour until the steady state value is

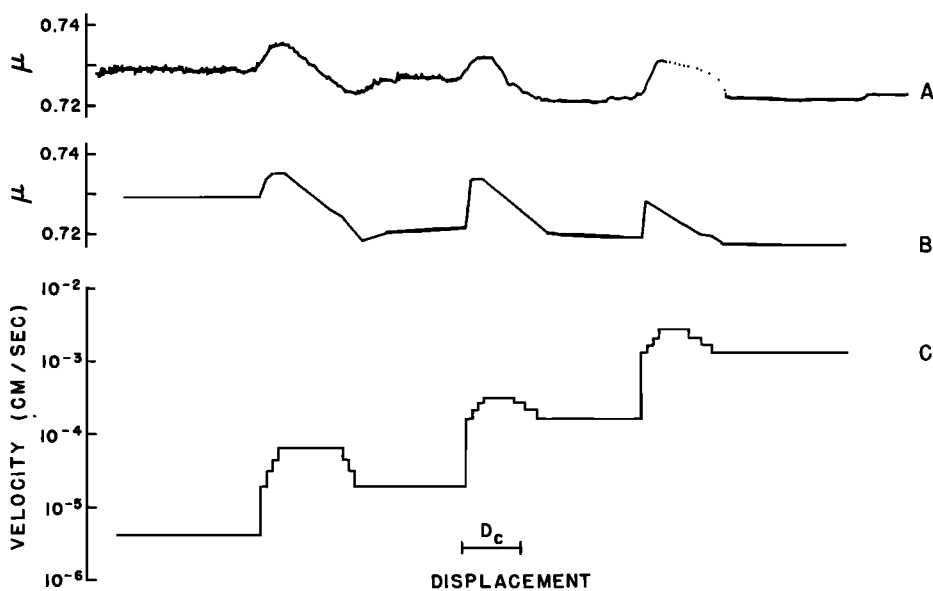


Fig. 4. Comparison of experimental results with empirical friction laws (9) and (11). Curves A and B give μ as a function of displacement, from the experiments of Figure 1 and for the model. Curve C gives velocity as a function of displacement used for the model.

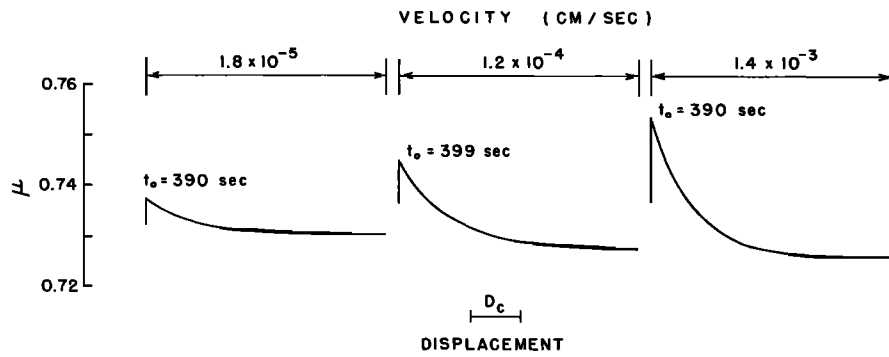


Fig. 5. Simulation of the experimental data of Figure 2. Friction parameters for (9) and (11) are $d_c = 2 \times 10^{-3}$ cm, $c_1 = 0.69$, $c_2 = 0.013$, $c_3 = 0.5$, $f_1 = 1.0$, $f_2 = 20.$, and $f_3 = 2 \times 10^{-3}$.

reached. If stress (μ) is held constant or allowed to decrease, then δ must decay with total elapsed time. The latter case corresponds to the creep observed in these experiments, Figure 2, and to the primary creep reported by *Solberg et al.* [1978].

Curves labeled by points *a-i* in Figure 6 show the approximate paths followed for the experiment of Figure 2. Point *a* in Figure 6 corresponds to the first peak in friction for slip at 1.8×10^{-5} cm/s. Contact time is approximately 400 s. As sliding progresses, μ decreases along the path *a-b* and stabilizes at *b*. Closure of the hydraulic valve prevents further slip at *b*. Any additional slip results in a decrease in stress in the sample which drops μ into the field below the dashed curve. Because δ is less than the steady state value, contact time increases along the path *b-c*. Assuming that slip is small during creep, displacement will not change the population of contacts significantly, and contact time will be approximately equal to the duration of creep. At *c* the valve is opened, and stress rapidly rises to the second peak, *c*, where the slip velocity is 1.2×10^{-4} cm/s. In response to slip, t and μ follow the path *d-e* and stabilize at *e*. Again at *e* the valve is closed, and creep occurs following the path *e-f*. Path *f-g* is the loading of the sample at a velocity of 1.4×10^{-3} cm/s, and *g-h* is slip at that velocity. Creep following closure of the valve follows *h-i*.

SUMMARY AND DISCUSSION OF SLIP INSTABILITY

Equation (11), used with (9), appears to give an adequate representation of the experimental observations reported here for the variation of friction with time, displacement, and slip

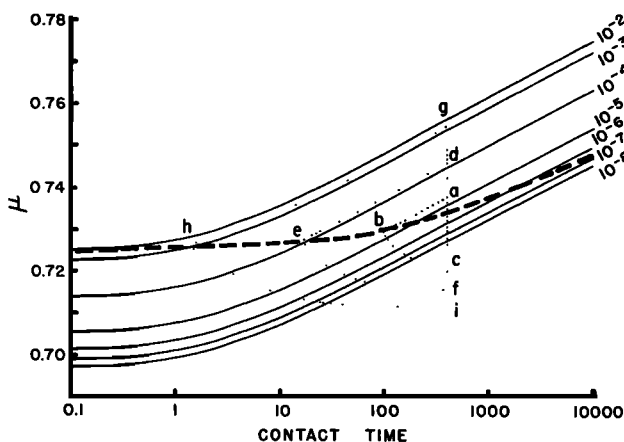


Fig. 6. Coefficient of friction versus time of contact, from (11) using the parameters given for Figure 5. The solid curves give instantaneous values of μ for different slip velocities (cm/s). The dashed curve gives μ versus t for steady state slip, $t = d_c/\delta$. The dotted curves *a-i* show the path followed by the experiment in Figure 2.

velocity. It is quite possible that other mathematical relationships could give as good a representation, or perhaps better, of the data. However, the results presented here clearly establish the qualitative effect of several experimental parameters affecting rock friction. Specifically, the coefficient of friction can be expressed as the product of the parameters *C* and *F*. Parameter *C* depends on the time of contact as given approximately by (7), and *F* depends on velocity of slip as given approximately by (10). During slip, time of contact is proportional to δ^{-1} , and for changes in velocity, t relaxes to a new value over the characteristic displacement d_c (equation (9)). For steady state slip the decrease in contact time with increasing velocity results in lower friction values at higher velocities. Hence there are two competing velocity effects. The first is a transient effect giving an immediate increase in friction for an increase in slip velocity. The second arises indirectly from decrease in contact time with increased velocity and becomes fully evident only after finite displacement at the new velocity.

The effect of contact time on friction apparently arises in response to normal stress which causes creep at contacting asperities, increasing the actual area of contact between the sliding surfaces or between particles of gouge along the surface. The transient velocity effect, the rate dependence of peak friction, and the decaying creep at subcritical stresses are caused by the velocity term in *F* and are identified here with a strain rate dependence in the shear strength of adhesive junctions at the points of contact. It is not clear what specific processes control failure of the contacts. Simple pulling apart of the adhesive junctions without surface damage, brittle failure of the contacting asperities, and ploughing may all be important processes. The presence of wear-generated gouge along the surfaces gives evidence for at least some brittle processes during slip. Hence in summary, the observations on time of contact suggest that creep determines the size, i.e., cross-sectional area, of the junctions that subsequently fail, at least in part by strain rate or velocity-dependent brittle processes.

These experimental results expand and clarify similar previous results [Dieterich, 1978b] and have some implications for the mechanics of unstable slip on simulated faults and for instability models of the earthquake source. On the basis of the earlier results, Dieterich [1978b] presents a simple spring and slider model for unstable slip based on displacement weakening and time dependence of friction. With this model the spring with stiffness *K* represents the combined stiffness of the sample and test apparatus. The friction of the slider is time dependent and velocity dependent, and the drop in stress $\Delta\tau$ from the static value to the sliding value is assumed to be linear over the displacement d_c . Unstable slip occurs when the decrease of frictional strength $\Delta\tau$ over the critical displace-

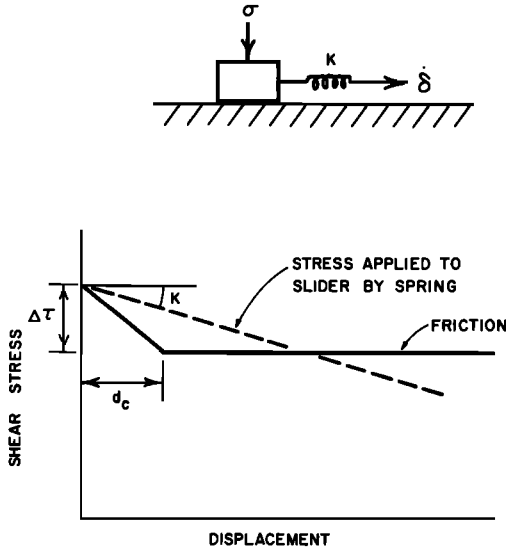


Fig. 7. Instability model.

ment d_c has a slope that exceeds the slope of the unloading curve of the spring, $-K$. In that case the stress applied to the slider by the spring exceeds the frictional resistance, resulting in an acceleration of the slider and instability (Figure 7). Hence for instability:

$$K < \Delta\tau/d_c \quad (12)$$

Stable sliding takes place if the decrease of friction with displacement has a lesser slope than K . The transition between the stable slip field and unstable field is where the slope of the unloading curve equals the slope for displacement weakening of friction:

$$K = \Delta\tau/d_c \quad (13)$$

Take

$$\Delta\tau = \Delta\mu\sigma \quad (14)$$

where $\Delta\mu$ is the change in the coefficient of friction, which would depend here on changes in time of contact and velocity of slip as given by (11). From (13) and (14),

$$K = \Delta\mu\sigma/d_c \quad (15)$$

for the transition from stable sliding to stick slip. Hence instability is highly machine dependent (K) and is controlled in addition by σ , d_c , and $\Delta\mu$. Relationship (15) was found to be in good quantitative agreement with experiments in which stiffness, normal stress, and d_c were all systematically varied [Dieterich, 1978b]. Low stiffness, high normal stress, and small d_c favor unstable slip. An implication of the model and constitutive equations is that $\Delta\mu$ depends on time of static contact and slip velocity. Large contact times combined with high loading velocities favor instability. Also the model indicates that a block that is experiencing stable slip can be induced to slide unstably if a perturbation increasing slip velocity results in a decrease in friction with displacement that exceeds the machine stiffness. This effect was frequently observed in velocity experiments of the type illustrated in Figure 1 when the velocity was increased by several orders of magnitude. This result suggests that faults with stable slip and few earthquakes, such as the central California portion of the San Andreas Fault, may have potential for instability in a large earthquake.

For more specific application to faulting and earthquake

instability, machine stiffness in the model must be replaced by the equivalent stiffness for slip on a fault. Following Walsh [1971], Dieterich et al. [1978] propose that for confined slip on a fault segment the effective stiffness is determined by the length L of the slipped zone as given by the usual fault displacement relationship

$$K = \frac{\Delta\tau}{d} = \frac{G}{\eta} \frac{1}{L} \quad (16)$$

where $\Delta\tau$ is the change of stress caused by the average slip displacement d on a fault of length L , G is the shear modulus, and η is a geometric constant with values near 1. Combining (12) with (16) gives

$$\frac{G}{\eta} \frac{1}{L} < \frac{\Delta\mu\sigma}{d_c} \quad (17)$$

for unstable slip. As in the case of the spring and slider model, high σ , high $\Delta\mu$, and low d_c all favor instability.

In addition, because effective stiffness is proportional to L^{-1} , large L favors instability. Conversely, the model predicts that for fixed d_c , $\Delta\mu$, and σ there will be a minimum fault dimension for unstable slip (i.e., a minimum earthquake). Experimental corroboration of the prediction of minimum fault dimension for instability is given by Dieterich et al. [1978], who observed, in a large-scale biaxial experiment (sliding surface, 200 cm), stick slip events confined to the central portion of the surface. In contrast, a nearly identical experimental configuration using fluid injection on a small block (sliding surface, 16.5 cm) produced only confined stable slip [Dieterich and Raleigh, 1974]. Parameters for these experiments are $\sigma = 5.0$ MPa, $\Delta\mu = 0.05$, $G \approx 2.5 \times 10^4$ MPa, and $d_c = 5 \times 10^{-4}$ cm, giving from (17) 50 cm as the minimum dimension for confined unstable slip.

For application to faulting it is of obvious interest to understand the parameters that control the scaling of d_c . At present, d_c appears to be independent of σ and shows a correlation with surface roughness. However, d_c may be controlled by gouge parameters instead, the roughness correlation arising only because of a control of gouge thickness or gouge particle size by roughness. The occurrence of small earthquakes may be used with (17) to obtain an upper limit estimate for d_c if earthquake stress drop is equated with the change in fault friction. For example, taking $L = 50$ m, $\Delta\tau = 1$ MPa, and $G = 2.5 \times 10^4$ MPa for earthquakes of magnitude ≈ 1 gives from (17) $d_c < 2$ mm. Because gouge zones are frequently orders of magnitude larger, this suggests perhaps that d_c may not scale simply as a function of gouge thickness.

Additional experiments are needed to explore the details of time, displacement, and velocity dependence as a function of rock type, pressure, and especially temperature. Generally, friction data in the literature are inadequate to test for the time, velocity, and displacement dependences reported here for normal stress above approximately 1 kbar. The similarity of observations for frictional instability for different types of rocks and for very different normal stresses suggests that the effects noted above are general characteristics of rock friction at room temperatures. Time-dependent effects that agree with the general form of (7) have been reported for normal stresses from 1.9 MPa to 70.0 MPa for a variety of rocks [Dieterich, 1972b; Teufel and Logan, 1978]. Evidence for the parameter d_c is limited and has been noted only in the study by Dieterich [1978b] and the present study. However, the model for the transition from stick slip to stable sliding by Dieterich [1978b]

Specifically requires a characteristic displacement and successfully accounts for data to normal stresses of 1.2 kbar. Data for the velocity dependence of the type given in (10) are reported here for the first time and need additional experimental corroboration. The similarity of the velocity dependence of F to the widely observed strain rate dependency of the brittle strength of silicates suggests that this effect will prove to be general.

Exclusive of specific constitutive properties or mechanisms controlling fault strength, the very occurrence of earthquakes on preexisting faults probably implies some qualitative constitutive effects of the type reported here. The line of reasoning leading to this conclusion is as follows: In general, earthquake instability theories require some type of displacement weakening to account for the loss of strength that occurs at the time of slip. As noted at the beginning of this paper, displacement weakening in turn requires that a healing process operate to restore the strength of the fault. Otherwise, repeated earthquakes could not occur without the strength eventually going to zero. The healing process seen in these experiments is apparently related to time-dependent creep at points of contact. Other healing processes that might be envisioned, involving consolidation, chemical processes, cooling, pore pressure equilibration, etc. are also time-dependent processes. Hence during slip there will be competition between the rate of loss of strength caused by displacement and the rate of increase in strength caused by healing. At low velocities of slip, healing will be more effective than at high velocities. As a result, velocity dependence, giving lower strength at higher velocities, will probably be important. As shown in the companion paper, velocity dependence used in a more general instability model than is considered here gives rise to interactions that may be important for understanding preseismic fault slip and the detailed process leading to instability.

REFERENCES

- Bowden, F. P., and D. Tabor, *The Friction and Lubrication of Solids*, vol. 2, Clarendon, Oxford, 1964.
- Brace, W. F., and J. D. Byerlee, Stick-slip as a mechanism for earthquakes, *Science*, **153**, 990, 1966.
- Brace, W. F., and J. D. Byerlee, California earthquakes: Why only shallow focus?, *Science*, **168**, 1573-1575, 1970.
- Byerlee, J. D., The fracture strength and frictional strength of the Weber sandstone, *Int. J. Rock Mech. Mining Sci.*, **12**, 1-4, 1975.
- Dieterich, J. H., Time-dependent friction as a possible mechanism for aftershocks, *J. Geophys. Res.*, **77**, 3771-3781, 1972a.
- Dieterich, J. H., Time-dependent friction in rocks, *J. Geophys. Res.*, **77**, 3690-3697, 1972b.
- Dieterich, J. H., Earthquake mechanisms and modeling, *Annu. Rev. Earth Planet. Sci.*, **2**, 275-301, 1974.
- Dieterich, J. H., Preseismic fault slip and earthquake prediction, *J. Geophys. Res.*, **83**, 3940-3947, 1978a.
- Dieterich, J. H., Time-dependent friction and the mechanics of stick-slip, *Pure Appl. Geophys.*, **116**, 790-806, 1978b.
- Dieterich, J. H., Modeling of rock friction, 2, Simulation of preseismic slip, *J. Geophys. Res.*, **84**, this issue, 1979.
- Dieterich, J. H., and C. B. Raleigh, A laboratory earthquake control experiment (abstract), *Eos Trans. AGU*, **55**(5), 353, 1974.
- Dieterich, J. H., C. B. Raleigh, and J. D. Bredehoeft, Earthquake triggering by fluid injection at Rangely, Colorado, in *Proceedings of the International Society of Rock Mechanics/International Association of Engineering Geology Symposium: Percolation Through Fractured Rock*, 12 pp., Deutsche Gesellschaft für Erd-und Grundbau, Stuttgart, West Germany, 1972.
- Dieterich, J. H., D. W. Barber, G. Conrad, and Q. A. Gorton, Preseismic slip in a large scale friction experiment, *Proc. U.S. Rock Mech. Symp. 19th*, 110-117, 1978.
- Johnson, T. L., A comparison of frictional sliding on granite and dunite surfaces, *J. Geophys. Res.*, **80**, 2600-2605, 1975.
- Raleigh, C. B., J. H. Healy, and J. D. Bredehoeft, Faulting and crustal stress at Rangely, Colorado, in *Flow and Fracture of Rocks*, *Geophys. Monogr. Ser.*, vol. 16, edited by H. C. Heard, I. Y. Borg, N. L. Carter, and C. B. Raleigh, pp. 275-284, AGU, Washington, D.C., 1972.
- Scholz, C. H., and J. T. Engelder, The role of asperity indentation and ploughing in rock friction, I, Asperity creep and stick-slip, *Int. J. Rock Mech. Sci. Geomech. Abstr.*, **13**, 149-154, 1976.
- Scholz, C. H., M. Wyss, and S. W. Smith, Seismic and aseismic slip on the San Andreas fault, *J. Geophys. Res.*, **74**, 2049-2069, 1969.
- Scholz, C. H., P. Molnar, and T. Johnson, Detailed studies of frictional sliding of granite and implications for the earthquake mechanism, *J. Geophys. Res.*, **77**, 6392-6406, 1972.
- Solberg, P. H., D. A. Lockner, R. S. Summers, J. D. Weeks, and J. D. Byerlee, Experimental fault creep under constant differential stress and high confining pressure, *Proc. U.S. Rock Mech. Symp. 19th*, 118-121, 1978.
- Teufel, L. W., and J. M. Logan, Effect of shortening rate on the real area of contact and temperatures generated during frictional sliding, *Pure Appl. Geophys.*, **116**, 840-865, 1978.
- Walsh, J. B., Stiffness in faulting and in friction experiments, *J. Geophys. Res.*, **76**, 8597-8598, 1971.

(Received April 18, 1978;
revised December 31, 1978;
accepted January 10, 1979.)